ISSN No:-2456-2165

Novel Cold Fusion Reactor with Deuterium Supply from Backside and Metal Surface Potential Control

Noriyuki Kodama
Studied Physics at Tokyo Institute of Technology (1983-1987),
Studying cold fusion as an independent researcher since 2020.
Sekido 5-2-7, Tama-city, Tokyo, 206-0011, Japan,

Abstract: - It is proposed that Cold fusion can occur in metal by D^+ hopping to T sites with D^- on the metal surface. In this mechanism, D^+ hopping is assisted by the Coulomb attractive force between D^+ and D^-, suggesting that control of the positive surface potential of the metal is important. D_2 thus formed at surface T site is compressed by T-site atoms due to the size difference between D_2 and the original T-site volume. Compression of the D_2 covalent bonds creates a small D_2 atom with Electron Deep Orbit (EDO) at a radius of a few femtometers, which is small enough to completely shield the Coulomb repulsive force between d-d and thus leads to the fusion. Hydrogen with DEO is verified by the experimental data of "high compressibility of hydrogen" and soft x-ray spectra which roughly matched the theoretical value of EDO. Because the current Cold fusion reactors are based on Fleischmann and Pons Effect (FPE), they have serious issues originating from voltage conditions of D absorption under the electrolysis condition which has the negative metal surface potential although the real Cold fusion needs the positive metal surface potential. Thus, it is very difficult to trigger fusion due to the voltage condition mismatch. Therefore, FPE needs a very high temperature by a strong local resistive heating of Pd Rod caused by the insulating film growth on fragments of Pd surface during D charging. The inhomogeneous insulating film growth is caused by very high electric field and by its variation caused by the Pt wire anode cage. Thus, I propose the novel Cold fusion reactor based on the real Cold fusion mechanism, with the proper metal surface potential control for D absorption and for Cold Fusion separately with very high surface potential uniformity, which fixes the most of the issues of reactors based on FPE. D supply from the backside of the reaction surface can eject ^{4}He at the surface T site, resulting in high excess heat generation. Because the total excess heat generation is determined by the D supply speed to the reaction surface of metal, D supply from the backside of metal is also needed to maximize the D supply speed, and Thus Ni-D layer deposition under the reaction surface is promising to have the larger excess heat generation because it has huge amount of D at the very close location to the reaction surface, like FPE.

Keywords:- *low energy nuclear reaction, LENR, Cold Fusion, Electron Deep Orbit, EDO, Coulomb Repulsive Force Shielding, Fleischmann and Pons Effect, FPE, Biological Transmutation.*

I. INTRODUCTION

1.1 Background

In 1989, Martin Fleischmann and Stanley Pons were catapulted into the limelight with their claim to have achieved fusion in a simple tabletop apparatus working at room temperature [1]. Their report described an experiment involving electrolysis using D_2O in which the cathode fused (melting point 1544 ºC) and partially vaporized, and the fume cupboard housing the experimental cell was partially destroyed.

After Fleischmann and Stanley's report, a substantial number of follow-up research was conducted to reproduce the reported FPE, however the reproducibility was low.

1.2 FPE Overview

Martin Fleischmann and Stanley Pons reported the abnormal heat generation of D_2O with Pd Rod under the electrolysis conditions reported in ref [1], which is now called "Fleischmann Pons Effect", or "FPE". Because the real Cold fusion needs the positive metal surface potential however FPE has the negative metal surface potential under the electrolysis condition. Thus, FPE differs from the real Cold fusion for the opposite voltage polarity to real Cold fusion.

Because of small number of experiments on the real Cold fusion, the understanding of FPE mechanism is important.

The experimental results on FPE replication are listed below:

(1) High D/Pd ratio is needed to generate the excess heat [1].
(2) Replication experiment by Takahashi [2] shows that Pd Rod with surface insulator [3], improves the excess heat generation by increasing the cell voltage.
(3) Surface nano roughness improves the excess heat generation.
(4) Nano-particle is used to improve the heat generation [4,5].
(5) Excess Heat generation occurs on the surface rather than bulk.
(6) The measurement in [6] shows that T site on the surface of Pd nanoparticle has larger D occupancy than that in the core region.
(7) The number of detected neutrons was nevertheless many orders of magnitude lower than what would be expected to explain the energy generation observed [7]. This is the main counterargument by skeptics of Cold fusion.

(8) The amount of 4He ash emission clearly correlates with total heat generation [8],[9], thus, the energy of 4He is transferred to the metal lattice and so the neutron and gamma ray emission are not always necessary and not detected actually. This is the answer to the counterargument of (7) and explained in 4.4.5.

1.3 Lattice confinement theory and Coulomb repulsive force shielding

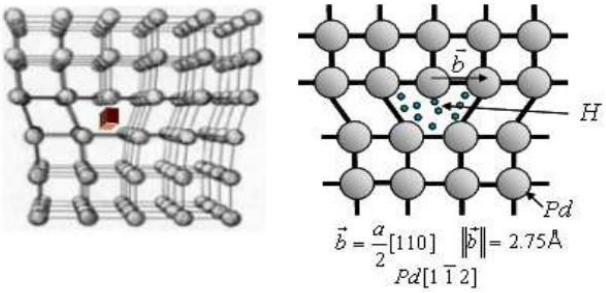

Fig.1. Scheme of edge dislocation loops in Pd containing condensed H/D. [10].

At the initial stage of FPE replication experiments, most of researchers proposed that the lattice confinement can cause the fusion for example as shown in Fig. 1 [10]. The authors developed a technique for embedding ultra-high-density deuterium clusters (D clusters) into Palladium (Pd) thin film and suggested that hydrogen in ultra-high-density clusters is confined in the dislocation which is created by a very high stress inside the metal and have the special state Rydberg matter [11]. However, the D cluster confinement in the bulk defects is inconsistent with other experimental data explained in 1.1.2.

All the similar confinement theories are based on the experimental evidence that a very high D/Pd ratio is required for FPE. Therefore, it would be reasonable assuming that so close d-d distance is possibly caused by the internal force in metal, therefore there are similar theories explaining the ultra-dense D clusters are related to the confinement in dislocations, defect or in lattice space. However, the estimation of the required force shows that according to the simple lattice confinement theory the d-d distance cannot be reduced to the fusion distance by external force as explained by Yu Fukai [12] as explained below.

To enable fusion, the distance between the nucleons should be shorter than the fusion distance (0.1-1 pm), so the Coulomb repulsive force at the fusion distance of 1.5 pm is calculated to be $1x10^{-6}$ N. However, the elastic induced stress in Pd is estimated to be at least two orders of magnitude smaller than that based on the Pd elastic constant. For example, as a typical internal stress in a metal is on the order of 10 GPa, the pressure applied to hydrogen atom can be estimated as 1 GPa = 10^9 N/m^2 = $1E^{-9}$ N/nm^2 = $1E^{-11}$ N/Å^2. Therefore, the $1E^{-6}$ N force needed to cause fusion is by 2-4 orders larger than the possible internal force in the metal estimated above.

Thus, the Pd lattice cannot provide the compression needed to shorten d-d to d_2 fusion distance, and another proper mechanism of Coulomb repulsive force shielding should be involved.

Therefore, I selected the non-standard model of hydrogen electron orbit which provides a possible answer as explained in section 3.1.

II. OVERVIEW OF THE COLD FUSION MECHANISM

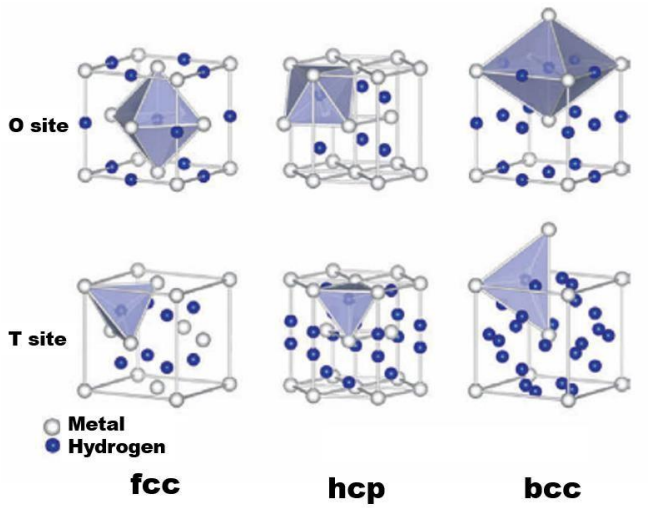

Fig.2. Types of metal lattices (O: octahedral sire, T: tetrahedral site).

The idea for the mechanism of Cold fusion presented here arose from the reviews on Cold fusion and FPE literature mentioned in 1.1.2 and in 1.1.3, EDO theory for complete Coulomb repulsive shielding, and research on metal hydrides, which together allude to hydrogen behavior in metals being the key to the occurrence of Cold fusion. A surprising fact that almost all Cold fusion phenomenon has been observed in fcc (and hcp) transition-metal hydrides and deuterides is mentioned in [13]. Because fcc and hcp have the closest packed structures shown in Fig. 2 and the FPE features (4) and (6) in section 1.1.2 indicate that the Cold fusion could occur at the surface T site occupied by D-.

Because the D absorption and Cold fusion must proceed under the different conditions, let's start with the stage when hydrogen storage is finished in Fig. 3(A).

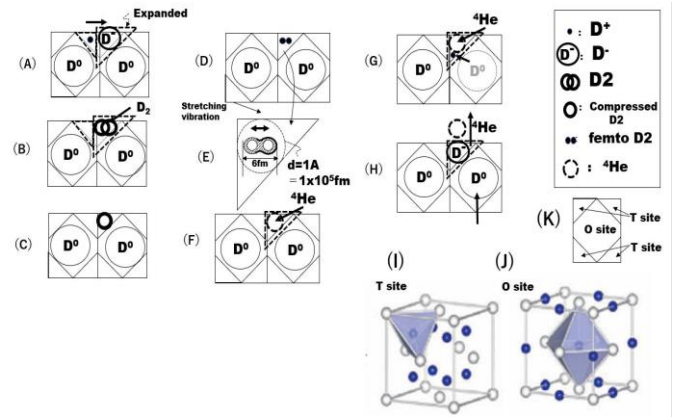

Fig. 3. Proposed Cold fusion mechanism.

(A) D^- in a surface T site and D^+ in an adjacent surface site. D^+ at surface T site tends to move to D^- at surface T site.
(B) T site occupied by D^- with subsequent D_2 formation by the hopped D^+ to T site occupied by D^-.
(C) D_2 compression.
(D)(E) D_2 transforms into a small D_2 with EDOs based on EDO theory.
(F) ^4He forms due to cold fusion.
(G) ^4He is ejected from metal by occupying another D^- at surface T site.
(H) D^+ turns into D^- to eject ^4He, and D^0 fills the unoccupied O site.

2.1 Step (A): D absorption

(1) D^- at the surface T site, D^0 in O site; Fig. 3(A);

The hydrogen nature in metals is explained in [14]-[24], and I would like to summarize here the nature of hydrogen in metals illustrated by Fig. 2 and 3. Hydrogen is H^0 at O site in Fig. 3, however, strictly speaking, hydrogen can be positive, neutral, and negative ion, depending on the electron exchange with the surrounding electronic state. In case of Hydrogen at T site, Hydrogen is negative (D^-) because it accepts the electron from the surrounding metal atoms due to their electronegativity. Due to the size difference between D^- and T site shown in Fig. 4 (the size of the T site is diameter=1.12 A, and the size of $D^-(H^-)$ is diameter<<4 A), thus hydrogen occupying T site expands the T site metal atoms. This is the cause of metal brittleness at a very high D/Pd ratio, and this expansion produces the compression stress at T site.

The recent theoretical calculations of the electronic structure of metal hydrides performed, founded by Switendick, have shown that both the H^+ or H^- models capture only one aspect of the facts [16]. Based on these features of hydrogen in metals it may comprise positive, neutral, or negative ion meaning that hydrogen has the resonance state between H^- to H^+. Therefore, the diffusion and status of hydrogen in the interstitials in metals need to be interpreted with the resonance, namely the charge of hydrogen can vary from negative (-1) to positive (+1) depending on the surrounding electronic state.

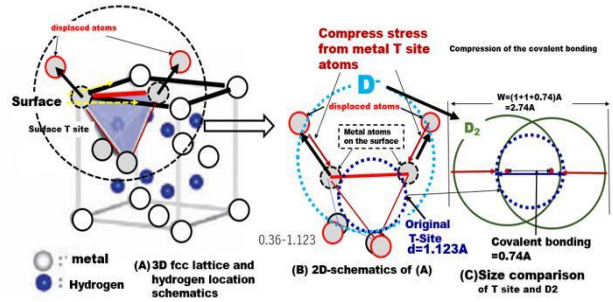

Fig.4. Pd surface T site atom expansion, and compression stress by T site atoms.

(A) 3D schematic of the surface metal atoms, and hydrogen at surface T site.
(B) 2D schematic with the scale adjusted to the 2D schematics from 3D schematics.
(C) 2D Schematic size comparison of D_2 and T site.

As is shown in Fig. 3(A), D can occupy the surface T site as D^- with the high priority due to the elastic surface lattice atoms on the surface as is shown in Fig. 4(A), (B). The size of H^- is determined by the minimization of the total energy of the displacement energy and the energy of hydrogen ion by the hydrogen charge change by the electron from surrounding metal atoms, thus the maximum size of H^- is the size of H^- in free space. The higher probability of the occupation at the surface T site was verified by the measurements in nanoparticles in ref [6].

2.2 Step (A)–(B): Hopping of D^+ to D^- at the surface sites

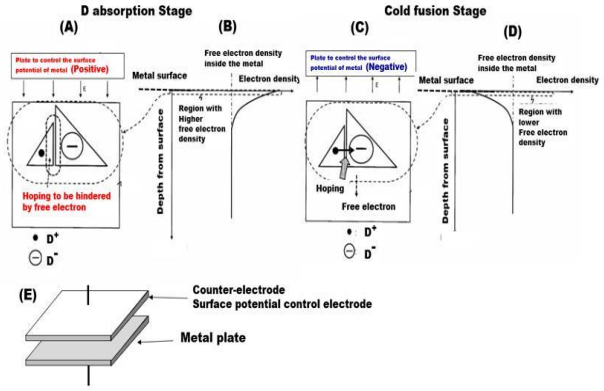

Fig.5. Proposed Cold Fusion Reactor to adjust the metal surface potential.

(A), (B) Metal surface potential control voltage is positive at the Cold fusion stage, the surface potential of metal is negative.
(C), (D) Metal surface potential control voltage at D absorption stage is negative, the surface potential of metal is positive.
(E) 3D schematic of the Cold fusion with the counter electrode and metal plate, which are the parallel plate electrodes.

Due to the opposite charge of D^+ and D^-, the ions attract, and at higher temperature D^+ moves to D^- in surface T site by

hopping and by Coulomb attractive force. Within the surface T site, D^+ and D^- form a D_2 molecule, as shown in Fig. 3(B). Coulomb attractive force shielding by free electrons in the region near the metal surface would hinder the hoping of D^+ to D^- in the adjacent surface T site as illustrated in Fig. 5(A), (B). In case of Cold fusion stage, the counter electrode voltage should be negative (Fig. 5(C), (D)) to positively charge the metal surface by the field induced charging by counter electrode. This hopping step could be promoted and well controlled by the parallel flat plates structure of counter electrode with negative voltage and grounded metal plate, see Fig. 5(E).

2.3 Step (B)-(C): Compressive stress from metal T-site atoms

The compression of D_2 is explained in Fig. 3(B-C). Based on the geometry of the fcc lattice parameters and the hydrogen ionic radius, see Fig. 4, the diameter of the inscribed sphere of the T site is 1.123 Å, the width of H_2 (D_2) is 2.74 Å, and the diameter of H^0 (D^0) is 2 Å, as shown in Fig. 4(C). The T site lattice atoms compress the D_2 molecules to make the d-d distance shorter by the compression of the D_2 covalent bonding. The D_2 molecule stretches and vibrates indicating the elasticity of covalent bonding Fig. 4 (C) demonstrates that the d-d distance can be zero without coulomb repulsive force. However, as explained in 1.1.3, the force keeping the d-d distance at fusion distance is large enough to prevent this. Thus, the proper Coulomb repulsive force shielding is needed to for the fusion. This can be achieved following the theory of EDO explained in sections 3.1 and 3.2.

2.4 Step (C) - (D): Creation of small D2 with EDO

This transition to small D_2 can be explained by the EDO theory, see section 3.1. This electron orbit located at a few femtometer distance from d can shield the Coulomb repulsive force perfectly as demonstrated in Fig. 6.

III. ELECTRON DEEP ORBIT (EDO) THEORY

3.1. Background of EDO

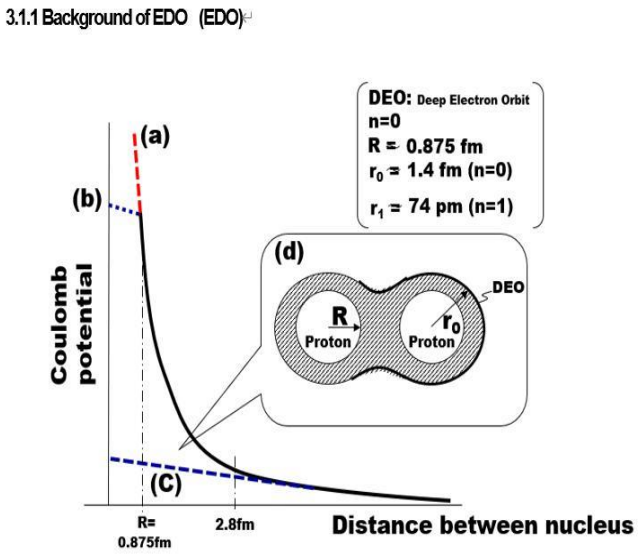

Fig.6. Coulomb potential of small hydrogen with EDO.

This section is based on the works [25]-[38], and the background of the study is described in [27]. Rutherford suggested already in 1920 that electron and proton could be tightly bound. After Chadwick's discovery of the neutron in 1932 there was a lot of discussions whether the neutron is an elementary particle or a hydrogen-like atom formed from electron and proton. The assumption that the small hydrogen is a neutron was finally rejected because the wave function is infinite at r = 0. Since nobody has observed it, the idea of the small hydrogen died. However, it revived again ~70 years later with the assumption that the proton has a finite size, and the electron experiences a different non-Coulomb potential at a very small radius [30,31]. The modified Coulomb potential is not infinite at r=0, because the positive charge is distributed within the nucleon uniformly as demonstrated in Fig. 6(b). Because of the very narrow orbit of a few femto meters from the nucleon, it has a perfect Coulomb repulsive force shielding and acts as a neutron shown in Fig. 6(c)(d).

In case of D_2, it should be a small D_2 molecule as shown in Fig. 6(d).

In [30], the authors explained that the existence of EDOs were predicted many decades ago following the Relativistic Klein–Gordon and Dirac equations. However, as the FPE and Cold fusion mechanism can be explained by the theory of EDO and small D_2 molecules, we must try to verify this by the measurements of soft X-ray emission spectroscopy, see sections 3.3.1-3.3.2

3.2 Experimental evidence of EDO of hydrogen

3.2.1 High Compressibility of hydrogen negative ion experiment

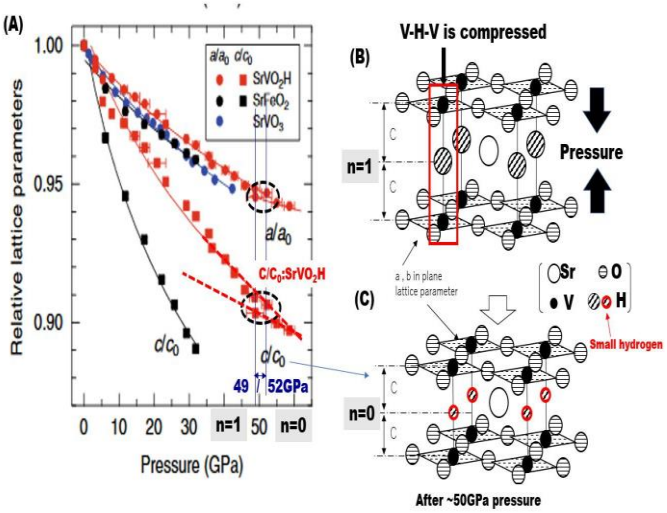

Fig.7. High-pressure behavior of SrVO2H and SrFeO [39].

(A)Pressure dependence of lattice parameters for the experimental (red) and the DFT-computed (sky blue) values of $SrVO_2H$ (note that some error bars are smaller than the width of the symbols). The decrease in pressure from 52 GPa to 49 GPa as the cell volume decreases suggests a phase transition to a denser phase. Relative lattice parameters, a/a0 and c/c0, of $SrVO_2H$ (red), $SrFeO_2$(black), and $SrVO_3$(dark blue) as a function of pressure.

(B)Schematics of $SrVO_2H$, and V-H-V bonding, which is compressed by the mechanical pressure.

(C)Schematics of $SrVO_2H$ under the 52 GPa pressure, illustrating the decrease in size of hydrogen negative ion.

Figure 7 is the experimental evidence of smaller hydrogen of the compressed V-H-V bonding [39]. The authors showed via a high-pressure study of anion-ordered strontium vanadium oxyhydride $SrVO_2H$ that H^- is extraordinarily compressible, and that pressure drives a transition from a Mott insulator to a metal at ~ 50 GPa. I think that this experiment is the direct evidence of the existence of EDO as discussed in 3.2.2. I would like to explain D_2 molecule case (D-D bonding) in the actual Cold fusion in place of V-H-V compression as is in Fig. 7(B)-(C).

3.2.2 Transition from D1s to D0s by the compression of D–D covalent bond

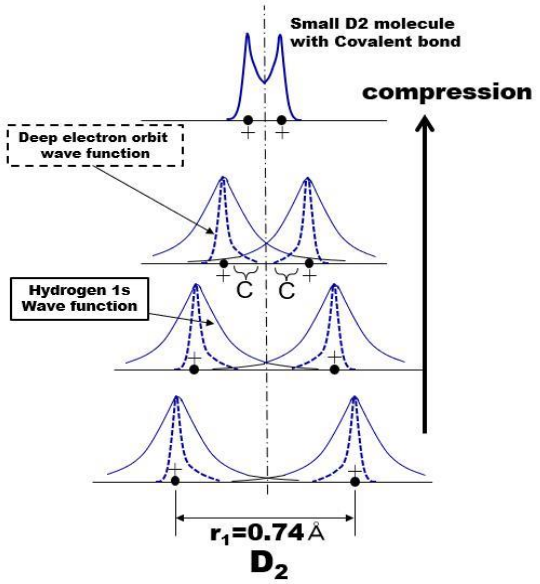

Fig.8. Mechanism of small atoms (molecules) generation by the compression of D-D covalent bonding.

The mechanism of electron transition to EDO proposed in this work is illustrated in Fig. 8. The size of D_2 at the surface T site is determined by the balance between the compression stress from the lattice metal atoms and the elastic rebound force of covalent bond and due to the nature of the covalent bonding the compression can cause the d-d distance shorter in d-d compression direction that brings two ds to be closer together in a collision direction.

Under compression of D_2 by external pressure, the d-d distance can decrease and the D_{1s} wave function tail can extend to overlap with the EDO wave function, which is localized at a distance of a few femtometers from the nucleus. Because the d-d distance is so small, the overlap (C in Fig. 7) of wave functions can be large enough to achieve a high tunneling probability of electrons from D1s to the EDO (D_{0s}). Radius of EDO is calculated to be few femtometers [30], [31], and is by far smaller than that of D_{1s} of 0.53 pm (Bohr radius). A small D2 molecule can be created due to the simultaneous transition of both D atoms to small D atoms, so D_2 molecule can transform to small D_2 molecule with the covalent electron at EDO as shown in Fig. 6(d).

3.3. Soft X-ray spectra measurements verifying the existence of the EDO

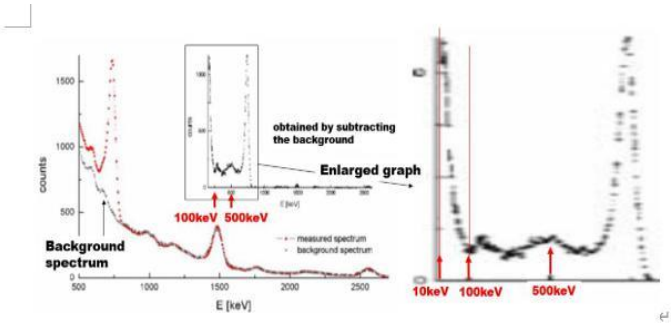

Fig.9. NaI γ-rays spectrum showing a peak superimposed to the background.

The insert, obtained by subtracting the background, shows the typical structure of a γ-ray: photoelectric peak, Compton and backscattering peak. In ref [40], Figure.7.

The direct evidence of EDO is to detect the soft-x-ray based on the theoretical calculation as follows. The theoretical calculation, which is now under study by Vavra Jerry and temporal results from the private communication shows that photons of these energies in case of relativistic Schrödinger equation are ~507.27keV, ~2.486keV, ~0.497keV or 0.213 keV, depending on which transition is involved. In case the Dirac equation, these energies are 509.13keV, 0.932keV, 0.311 keV, 0.115keV or 0.093keV, again it depends on which transition is involved. Ref [40] has an overview of our experimental activity during the last twelve years. They have been studying the Ni-H system at temperatures of about 700 K. Their investigations have revealed several interesting effects: (a) energy production for long time (b) neutron emission (c) γ-ray emission (d) charged particles emission (e) appearance of elements other than Ni on the surfaces of Ni samples.

These experiments were performed in several laboratories and tool configuration is the best as far as I know, so I think that reproducibility is excellent and it is very accurate. They performed at about 700K, which may not be the real cold fusion but FPE as is discussed in 4.1, and 4.4.5, so the result may have the gamma emission and neutron emission due to the higher temperature.

As is shown in Fig.9 the soft x-ray spectra has the broad peak at 500keV and sharp single peak at less than 100keV, and one small peak at around 100-200keV. Note that 500keV Peak is broader than peaks at less than 100keV, probably because of the orbit difference effect of EDO of hydrogen, and theoretical calculation roughly matches the measured x-ray spectra except the border peak at 500keV, which is discussed in 3.3.3 for the further study of the nuclear physics.

3.4. Proposed new set-up to detect soft X-ray spectra from Cold fusion

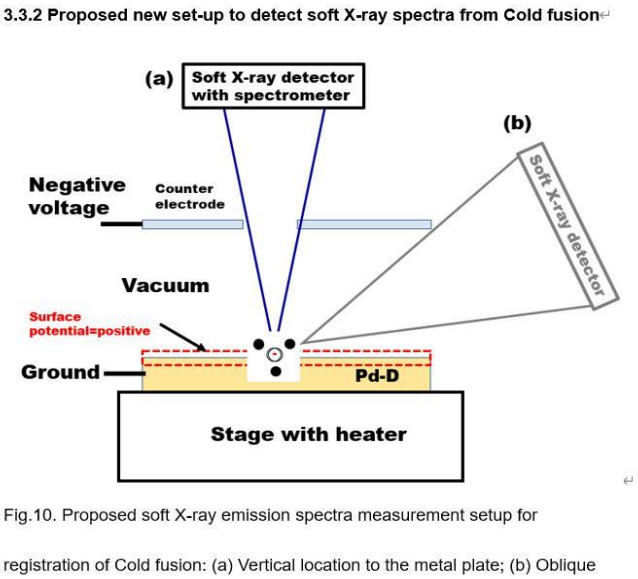

Fig.10. Proposed soft X-ray emission spectra measurement setup for registration of Cold fusion: (a) Vertical location to the metal plate; (b) Oblique

Fig.10. Proposed soft X-ray emission spectra measurement setup for registration of Cold fusion: (a) Vertical location to the metal plate; (b) Oblique location from metal surface.

I would like to propose a new experimental setup for soft X-ray spectra evidencing the Cold fusion mechanism (Fig.10(a)),

Because the Cold fusion is the surface reaction which occurs at the surface T site, and a positive surface potential is needed, the detector location is important because and metal atoms existing around the D_2 may shield the X-ray emission from D2 as shown in Fig. 10(b), and cooling down the metal temperature is important to run the real cold fusion operated at lower temperature to avoid neutron and gamma ray emission.

3.5. Possibility to cause the broader soft-x ray profile by the non-true sphere proton shape based on the proton shape measurement.

I would like to discuss here on the cause of this broad peak at 500keV.

As is explained in Historical background of Neutron is explained in 3.1.1, Rutherford suggested already in 1920 that electron and proton could be tightly bound. The assumption that the small hydrogen is a neutron was finally rejected because the wave function is infinite at r = 0. Since nobody had observed it, the idea of the small hydrogen died. However, r=0 issue was fixed by the practically modified coulomb potential, and more importantly I show that the Cold Fusion is real and is caused by EDO, based on the matching of soft-x-ray to the theoretical calculation and high compressibility of hydrogen.

More precisely I would like to discuss the cause of broader peak at 500keV.

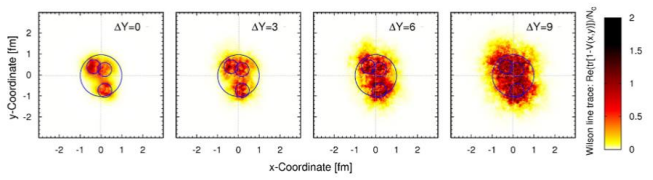

Fig.11. Transverse profile of a single proton configuration at four different intervals dY of the evolution.

The different panels show a contour plot of the real part of the trace of the Wilson line as a function of the transverse coordinates x and y. The small (large) circles show the position and size of the three constituent quarks (the proton). In ref [41], fig.1.

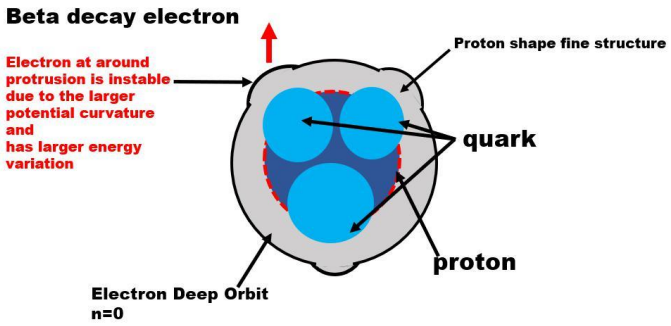

Fig.12 Schematics of proton shape with fine structure by three quarks and Electron Deep Orbit deviation

Figure 11 is the proton shape measurement results in ref [41] and this measurement suggested that there is a possibility of proton to have the fine structure by quarks, so it has the great impact on the deepest orbit energy as is shown in fig.12.

Because the soft x-ray spectrum study in 3.3.1, Fig.9 shows that 500keV(transition to the deepest orbit) has the broader peak than other orbit, I think that the closest electron deep orbit (r=a few fm) to the nucleus of d must have the very large variation of orbit due to the proton shape deviation from true spheric shape probably caused by three quarks from true sphere, and 500eV broad peak can be qualitatively explained by larger variation of orbit and energy in the deepest orbit caused by the fine structure by three quarks.

Therefore, because peak energy matches with the theoretical value and the deepest orbit have the broader peak than others, these soft x-ray peak result proves existence of Electron Deep Orbit of nucleus.

IV. MECHANISM OF FPE (COLD FUSION UNDER ELECTROLYSIS CONDITIONS)

4.1. Replication experiment

Replication experiments using a Pd sheet cathode centered within a Pt-wired anode in a D_2O/LiOD electrolyte were conducted by Takahashi et al, [2]. An anomalous heat excess was first observed, and later it was replicated with a much smaller excess heat level.

ISSN No:-2456-2165

To investigate the reproducibility, the second experiment was performed over 4 months with minor changes to the cell design. The excess heat was reproduced, but at much smaller level.

The authors noticed that the cell voltage in first experiment is anomalously high (~25 V in the beginning and up to ~30 V in the end) compared with those in 2nd Experiment (~14 V in the beginning and very slowly increase up to 20 V after 3 months). This replication experiment showed that the first experiment had much smaller "effective" surface area of Pd cathode than that in the second experiment. The surface analysis of Pd cathode in the first experiment showed the presence of Al-27 and Ca-40 deposits in amounts comparable to that of Li-7. This film can be formed by a high electric field strength of 10^6 V/cm assisted passive film growth [9]. It was proposed that the thin film grown on Pd surface may play a role of a "current blocking layer" enhancing the cathode over-potential (hence the cell voltage) and increase the cell current resulting in the higher resistance on the current path of Pd.

4.2. Mechanism of FP effect

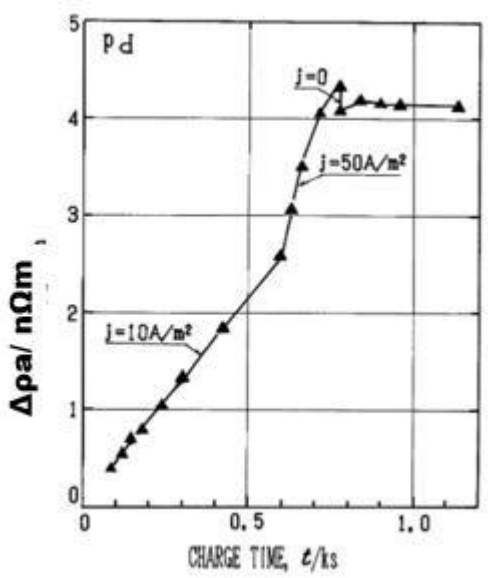

Fig.13. Resistivity increases due to dissolved hydrogen during electrolytic charging at 273 t/ks in ref [42]

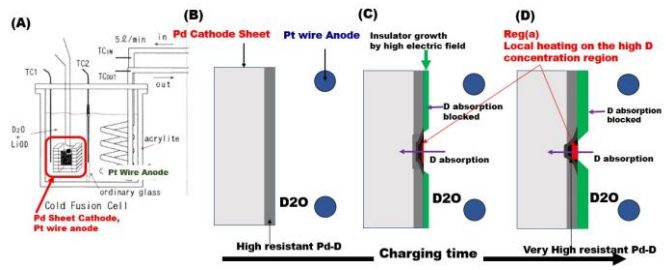

Fig.14. Schematics of FPE mechanism: (A) Experimental setup of Cold fusion cell; (B)-> (C) ->(D) charging with D and evolution of insulator growth.

As is shown in Fig.13, the resistivity increases with longer D charging time [42].

I would like to propose my mechanism of FPE based on the replication experiments in [2],[3], and based on the real Cold fusion mechanism, the Pd-D resistance change in Fig.13. The mechanism schematics is presented in Fig.14.

Following the replication experiments by Takahashi and the resistance change of Pd-D by Arai et al the sample with better excess heat and higher cell voltage contains the insulating film at Pd rod under the electrolysis conditions. Thus, I think that longer time of D charging causes the higher D concentration, and causes the higher resistance in Reg(a) in Fig.14. The insulating film grown under the high electric field cuts the current path and D diffusion into Pd Rod, therefore the D diffusion proceeds only in the region without the insulating film (Reg(a)). Note that the inhomogeneity of electric field created by Pt wire anode causes the inhomogeneous deposition of the insulating film on Pd Rod. So, the narrower current path and higher resistance of the openings (Reg(a)) in the insulating film on Pd Rod can cause the higher cell voltage due to the constant current mode and positive feedback of higher resistance and higher cell voltage to keep the current constant. Hence, the resistance can be rapidly so high that the local heat generation by higher resistance in Reg(a) in Fig.14 triggers the Cold fusion, because a very high local heat can cause the higher possibility of D^+ hopping and can increase the possibility of fusion. Once the fusion occurs locally, the metal temperature increases rapidly and causes a higher fusion probability and the positive feedback resulting in the fusion in all of region with the high Pd-D on Pd Rod.

The issue of irreproducible excess heat generation on FPE can be caused by the very high stress in the grown insulating film as shown in [3], because, as the author mentioned, the variations in electrode potential (open-circuit conditions), or current density (potentiodynamic scans) can be simply explained by a high field strength of 10^6 V/cm) assisted the passive film growth. Thus, the cold fusion reactor electrode geometry and configuration among Cold fusion reactors based on FPE are shown in Fig.15.

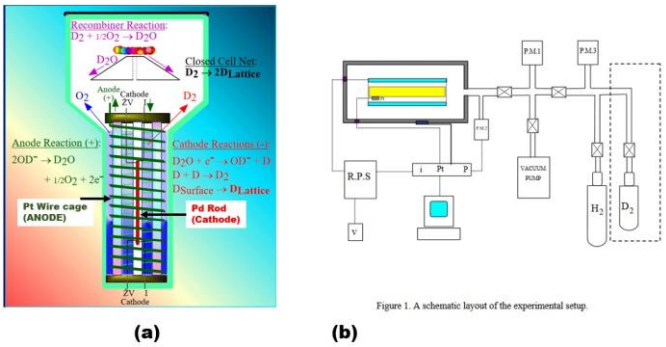

(a) (b)

Fig.15. Typical Cold fusion reactors (a)in ref [43], (b) in ref [41]

The electrode geometry and overall configuration of all of the current Cold fusion Reactors based on FPE are similar to the original setup [1] as is shown in Fig.13(a). FPE is not the real cold fusion from the engineering point of view because it has the issue of the high temperature triggering and irreproducibility owing to the simultaneous D absorption and

Cold fusion on the same surface, and inhomogeneous electric field by Pt wire and Pd Rod as is shown in Fig.13. so the proper design is needed to have the uniform electric field and to separate the Cold Fusion and D absorption to ensure stable and reproducible excess heat generation. The reactor in Fig13(b) in ref [41] has cylindrical sample or planar sample, so the electric field and metal surface potential seems to be uniform, and as far as I know, this is the best reactor. Thus, I would like the researchers using this type of reactor to run experiment on the potential impact on excess heat generation of cold fusion step as is shown in Fig.5.

Due to the low efficiency of the original setting of D2O electrolysis reactor based on FPE, the most researchers are using D2 gas to load hydrogen in metal, however D_2 gas method may be reconsidered because D_2 gas has the lower specific heat so the heat transfer efficiency seems to be lower than coolant of H_2O.

Thus, in section 5, I propose the novel design of Cold fusion reactor based on the real Cold fusion mechanism.

4.3. FPE using RF input

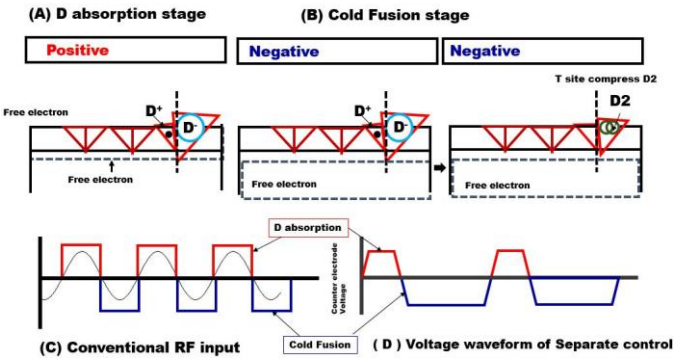

Fig. 16. Mechanism of Cold Fusion at RF Electrolysis:
(A)D absorption and
(B) ColdFusion stages;
(C)Conventional RF plasma voltage waveform;
(D) Proposed Separated control of D absorption and Cold fusion.

In [44], a new Cold fusion technique by Plasma Electrolysis is presented. The authors suggested that Plasma was formed on the electrode surface, and the measured heat exceeded the input power substantially by up to 200% in some cases. The reproducibility was 100%.

However, I do not think that plasma can form in the electrolysis with hydrogen storage metal electrode, and this excellent performance and high reproducibility are attributed to the separation of D absorption and Cold fusion in time as shown in Fig.16. Thus, this experiment evidences that the Cold fusion mechanism is related to the control of the metal surface potential. Note that adjusting the pulse voltage is important to optimize the excess heat generation as shown in Fig.16(D).

4.4. FPE advantage to eject 4He with D supply from the backside

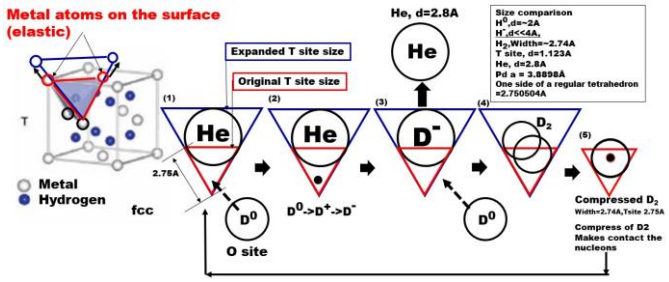

Fig. 17. Mechanism of 4He ejection from a surface T site

The very high D/PD ratio can produce the larger excess heat because of the large total amount of D accumulated in Pd Rod. But note that ^{4}He ash confined at surface T site can hinder the D absorption from the front surface, but in FPE D is supplied to the surface T site from the bulk, and ^{4}He ash is ejected from there as shown in Fig.15.

However, the way of switching the D absorption and Cold fusion has the issue of the remaining ^{4}He ash on the surface T site due to the limited D supply from the backside, Thus I think that D absorption and Cold fusion need to be separated. For the RF input technique wastes the times while D absorption step and the accumulation of ^{4}He at surface T sites hinder the D absorption.

4.5. Neutron and gamma ray emission, and energy transfer to the metal lattice in FPE

We had a lot of discussion whether Cold fusion is real, and why it is not accompanies by the neutron and gamma ray emission. Skeptics insist that Fusion requires the large dose of neutrons and gamma-rays to transfer heat to the metal lattice, however they completely misunderstand the Cold fusion and FPE mechanism. They suggest on the hot fusion reaction path as below:

$D+D \rightarrow [4He^*]\tau \sim 10\text{-}21s$

1. ^{3}He(0.8MeV) +n(2.45MeV): ～50%
2. T(1MeV) + p(3MeV): ～50%
3. ^{4}He(76keV) +γ(23.8MeV): ～10-5%

Note that above reaction channel occurs via the excited state of ^{4}He under the hot fusion conditions, however, Cold fusion occurs by small atoms or small D_2, so no extra energy is needed and the reaction is softer than hot fusion. In opposite, FPE sometimes needs a very high temperature to trigger the fusion, and in such case ^{4}He can have a larger energy and may emit neutrons and gamma rays. The heat transfer can be done via the ^{4}He energy based on lattice confinement [8],[9], and the heat transfer to H_2O coolant can proceed by hot ^{4}He ejected from the surface T sites. Therefore, the heat generation efficiency is very high because the D supply can be maximized.

V. A CONCEPTUALIZED COLD FUSION REACTOR

5.1 A Cold fusion reactor with D supply from the backside

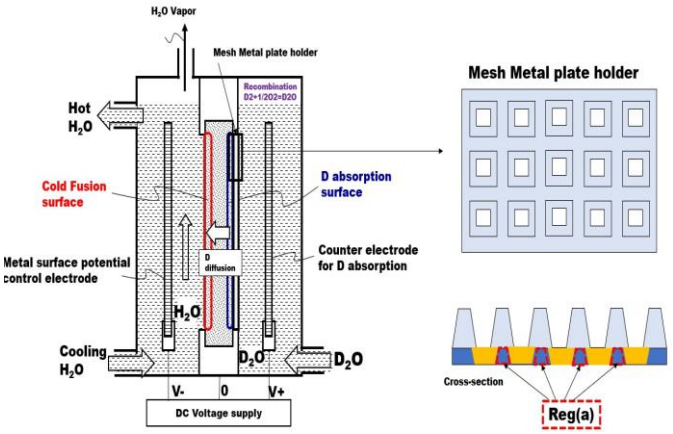

Fig.18. Conceptualized Cold fusion reactor with D supply from the backside.

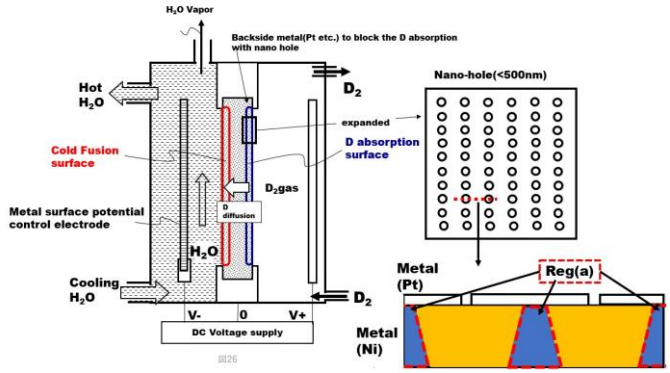

Fig.19. A conceptualized Cold fusion reactor of D supply from the backside by D_2 gas.

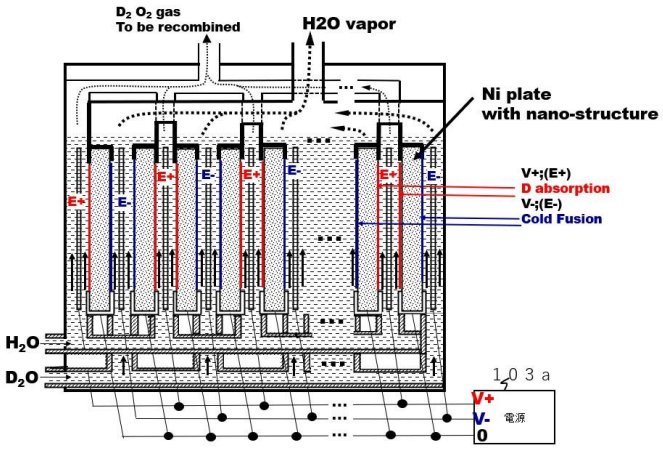

Fig.20. Cold fusion reactor having the multiple metal plates

The setup contains the mesh electrode which holds the metal plate and partially covers the D absorption area, but only the mesh window region of the metal plate may absorb D, whereas Reg(a) in Fig.18 and in Fig.19 around the center of the mesh frame has a very low D concentration. This is a rigid and low-resistance region to tightly control the potential of the cold fusion side of the metal and support the brittle metal to avoid cracking.

Because ^{4}He is confined in surface T site after d-d fusion, the total number of unoccupied surface T sites is decreasing with time. Thus, ^{4}He in surface T site must be ejected, while D absorption from the backside of the metal plate leads to the ^{4}He ash eject as shown in Fig.17, like in FPE.

Fig.19 represents a similar concept of D supply with D_2 gas from the nanoholes on the backside metal because D diffusion is limited in case of D_2O electrolysis condition owing to the insulator growth under the high stress, which blocks the D diffusion.

The very high-power burst of FPE can be attributed to the larger amount of D stored in the bulk metal region, which can supply D from the backside, thus in this reactor D is supplied from the backside and Cold Fusion occurs on the front side simultaneously, with a high D supply rate with D_2 gas (Fig. 19). If more power is needed, the cold fusion reactor may have the multiple metal plates as shown in Fig.20.

5.2 A new concept of Cold fusion reactor with Nano-Corn nanostructured metal Line and Space aligned along the H_2O coolant flow.

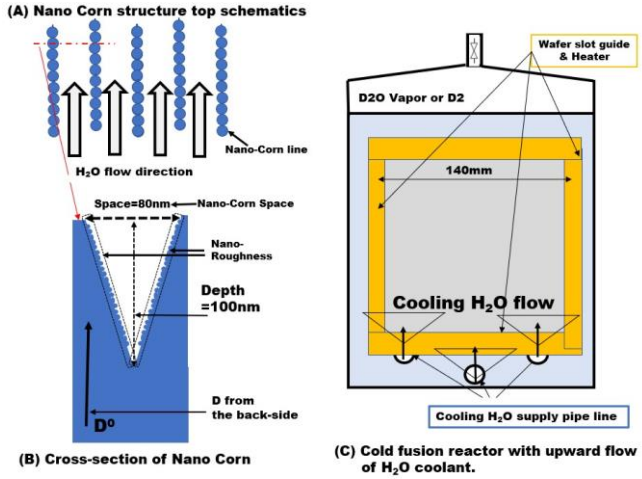

Fig. 21. Cold fusion reactor containing the metal Nano-Corn structure aligned along the H_2O coolant flow.
(A) Nano Corn structure top schematics.
(B) Cross-section of Nano Corn.
(C) Cold fusion reactor with upward flow of H2O coolant.

As shown in Figs.18,19,20,21, the H_2O coolant flows upward in the separated Cold fusion side. In Fig.21, the metal plate has the nanostructured pattern of Line/Space comprising the vertical nano-corn structure, which side wall is shown in Fig. 21(a), (b). It has the same effect on cold fusion as nanoparticles, and this reactor can precisely control the surface potential of nano roughness on nanopatterned surface on the positively charged side to improve the cold fusion efficiency.

ISSN No:-2456-2165

The side view of the reactor is presented in Fig. 21(c). The upward flow of the H_2O coolant along the Line/Space pattern to wafer with Line/Space with nanostructured pattern enhancing the H_2O flow rate, see Fig. 21(A) and (C). The pattern designed by a nano-imprinting technology provides the increase of the wafer surface area by 6 times compared to the surface area without the pattern. The experimental prototype design is now under discussion with a nanoimprinting tool vendor, so the experimental setup is not yet completed. [45]

5.3 A Cold fusion reactor with D supply from the Ni-D layer on the backside

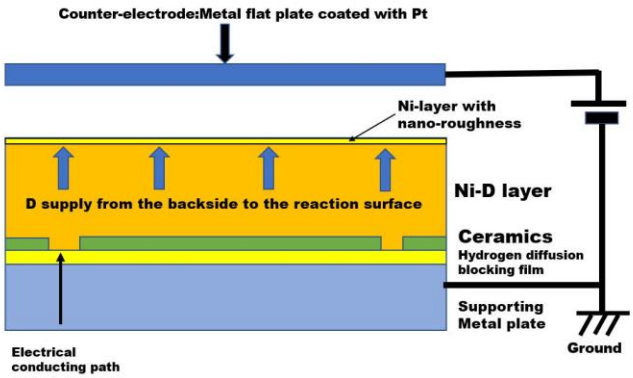

Fig.22. Cold Fusion reactor with D supply from the Ni-D layer on the backside of reaction metal layer

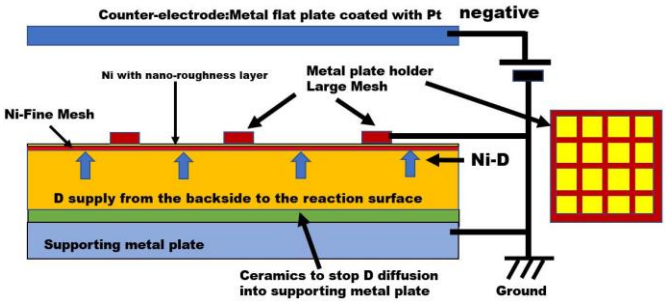

Fig.23. Cold Fusion reactor with D supply from Ni-D layer on the backside of reaction metal layer with nano-mesh and with metal plate holder on the front side of the metal

Because the excess heat generation is determined by D supply to the reaction surface and the number of reaction site at surface T site, and so the capture rate of D at the surface T site is also important as well as the total surface area.

High D concentration of Ni-D layer is deposited under the reaction surface, and this Ni-D is formed at the proximity of reaction surface to maximize D supply and to make the D loading time unnecessary.

To increase the capture rate Ni layer with nano-roughness is needed on the larger surface area, so Fig.23 use the fine Ni-mesh to increase the surface area and Ni deposition with nano-roughness can improve the D capture rate.

Figure 22 shows that the reaction metal surface has the electrically contact through hole on the ceramics or conductive ceramics, and the ceramics can stop D diffusion to the supporting metal side.

Figure 23 shows the metal structure with fine mesh to increase the surface area on the front side of the metal and Ni is sputtered with nano-roughness to increase the capture ratio of D at surface T site. Electrical connection to metal surface is from the metal plate holder on the front-side of the metal.

VI. BIOLOGICAL TRANSMUTATION

6.1.1 Background

The biological transmutation has the same mechanism of Cold fusion, So I briefly discuss its the mechanism as an additional evidence of the Cold fusion mechanism. It is shown that transmutation by Cold fusion was reported by several researchers with a high reproducibility, however the proposed mechanism of this phenomenon was not correct.

It is well known that in biological systems chemical elements can be transmuted into other elements [46]. Although these facts have been established since the early 19th century, they have been ignored by established science ever since. In [47], the author reported that femto atoms may cause the transmutation.

6.1.2 Category of biological transmutation based

I categorized the types of biological transmutation based on the report [48,46] as follows:

(1) Adding one proton (adding atomic nucleus of Hydrogen)

$^{39}_{19}K+1p=^{40}_{20}Ca$, $^{137}_{55}Cs+1p=^{138}_{56}Ba$

(2) Adding 6*proton+6*neutron (adding atomic nucleus of ^{12}C)

$^{28}_{14}Si+^{12}_{6}C=^{40}_{20}Ca$,

As shown above, the biological transmutation can be caused by the compression of the M-C and M-H (carbide and hydride) bonds to create small carbon or small hydrogen shielding the Coulomb repulsive force between M and H, or C. by the femto atom formation based on the mechanism of transmutation in ref [47]

6.1.3 Compression mechanism in biological systems

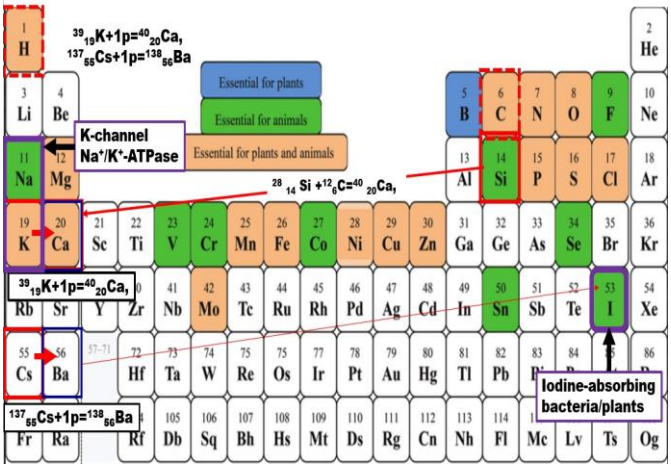

Fig.24. Periodic table with the essential elements for plants and animals.

ISSN No:-2456-2165

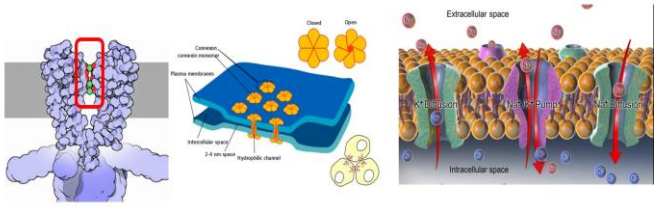

(A)Potassium channel (B) Gap Junction (C) Na^+/K^+-ATPase

Fig.25. Mechanism of bonding compression of carbide and hydride.
(A) Potassium channel, in ref [48].
(B) Gap Junction, in ref [49].
(C) Na^+/K^+-ATPase, in ref [50].

Figure 24 shows that there are essential elements between element to be transmuted and transmuted element, which indicates that mechanism to incorporate essential elements causes the biological transmutation.

Biological systems have the mechanisms to incorporate the essential element as is shown in Fig.25, Such mechanisms are Na-K pumping (Na^+/K^+-ATPase) [50], Potassium Channels [48], and gap junction [49]. It seems reasonable that such biological mechanisms to incorporate the essential element can compress the hydride (H-M bonding) and carbide (C-M bonding) to transmute mother element, M.

VII. SUMMARY

It is proposed that Cold fusion in metal is caused by the formation of small D_2 molecules with EDOs created by the compression of D_2 at surface T sites of close-packed metal structures. However, the FPE mechanism is different from the mechanism of real cold fusion, because in FPE D is absorbed under the electrolysis conditions in D_2O, under the voltage sign opposite to the real Cold fusion condition. EDO is proved by "High Compressibility of hydrogen negative ion experiment", and experiment on Soft-x-ray spectra during Cold Fusion, which peaks roughly match the theoretical calculations. A Cold fusion reactor based on this real cold fusion mechanism is proposed and the patent is pending at Japan Patent Office in [51],[52] The invention is the reactor where the Cold fusion and D absorption are spatially separated on the front/backside of the metal plate, respectively. The D absorption and Cold fusion can proceed simultaneously, and also can eject ^4He ash confined at the surface T site, resulting in the larger excess heat generation.

Another novel feature of the proposed Cold fusion Reactor comprises the nano-patterned metal plate, which is efficient to produce excess heat in the nano roughness on the sidewall of the nano-patterned metal structure and is efficiently cooled by the supplied H_2O coolant.

ACKNOWLEDGMENT

I would like to thank Vavra Jerry and Jean-Luc Paillet for useful discussions on EDO.

REFERENCES

[1]. M. Fleishmann, S. Pons, electrochemically induced nuclear fusion of deuterium, *J. Electroanal. Chem.* **261** (1989) 301-308, Also available from http://www.tuks.nl/pdf/Reference_Material/Cold_Fusion/Fleischmann%20and%20Pons%20-%20Electrochemically%20induced%20nuclear%20fusion%20of%20deuterium%20-%201989.pdf

[2]. A. Takahashi, A. Mega, T. Takeuchi, H. Miyamaru and T. Iida, Anomalous excess heat by D2O/Pd Cell under L-H mode electrolysis, *Third International Conference on Cold Fusion "Frontiers of Cold Fusion*". Nagoya Japan: (Universal Academy Press, Inc., Tokyo, Japan, 1992). Also available from https://www.lenr-canr.org/acrobat/TakahashiAanomalouse.pdf.

[3]. R. Salot, F. Lefebvre-Joud, Electrochemical behavior of thin anodic oxide films on Zircaloy-4, role of the mobile defects, *J. Electrochem. Soc*., **143** (12) (1996) 3902-3909. http://bbaroux.free.fr/recherches/publis%20selection%20av%202004/1996_JECS_Salot_Zirc.pdf

[4]. T. Mizuno, Method of controlling a chemically-induced nuclear reaction in metal nanoparticles, *ICCF18 Conference*, July 2013, University of Missouri. Addendum with new data, November 2013, Also available from https://www.lenr-canr.org/acrobat/MizunoTmethodofco.pdf

[5]. G.H. Miley, X. Yang, K.-J. Kim, E. Ziehm, T. Patel, B. Stunkard, A. Ousouf, H. Hora, Use of D/H clusters in LENR and recent results from gas-loaded nanoparticle-type clusters, *J. Condens. Matter Nucl. Sci*. **13** (2014) 411–421. Also available from http://coldfusioncommunity.net/wp-content/uploads/2018/07/411_JCMNS-Vol13.pdf

[6]. H. Akiba, M. Kofu, O. Yamamuro, Neutron diffraction of nano-crystalline PdD, *J. Jpn. Soc. Neutron Sci*., **27**(3) (2017). Also available from https://www.jstage.jst.go.jp/article/hamon/27/3/27_95/_pdf/-char/en

[7]. N. Oyama, O. Hatozaki, Present and future of cold fusion, *Oyo Buturi*, **60** (1991) 220-226. Also available from https://www.jstage.jst.go.jp/article/oubutsu1932/60/3/60_3_220/_article

[8]. L.F. DeChiaro, Low Energy Nuclear Reactions (LENR) phenomena and potential applications, NSWCDD-PN-15-00408; Distribution A: Approved for Public Release: Distribution is Unlimited, slide-10. Also available from http://fusion4freedom.com/science/navylenr.pdf.

[9]. M.C.H. McKubre, Review of experimental measurements involving dd reactions, Presented at the *Short Course on LENR for ICCF*—10, Slide-30, Also available from https://www.lenr-canr.org/acrobat/McKubreMCHreviewofex.pdf.

[10]. G.H. Miley, X. Yang, H. Heinrich, K. Flippo, S. Gaillard, D. Offermann, D.C. Gautier, Advances in proposed D-cluster inertial confinement fusion target, The Sixth International Conference on Inertial Fusion Sciences and Applications, *J. Phys., Conference Series*

244 (2010) 032036. Also available from https://iopscience.iop.org/article/10.1088/1742-6596/244/3/032036/pdf..

[11]. L. Holmlid, S.Z. Gundersen, Ultradense protium p(0) and deuterium D(0) and their relation to ordinary Rydbergmatter: A review, *Phys. Scr.* **94** (2019) 075005(26pp). Also available from https://iopscience.iop.org/article/10.1088/1402-4896/ab1276/pdf.

[12]. Y. Fukai, Review of cold fusion, *J. Phys. Soc. Japan*, **48** (1993) 354-360. Also available from https://www.jstage.jst.go.jp/article/butsuri1946/48/5/48_5_354/_pdf/-char/ja

[13]. H. Physics of the cold fusion phenomenon, *Proc. 13th International Conference on Cold Fusion*, Sochi, Russia, 2007. Also available from https://www.researchgate.net/profile/Hideo_Kozima/publication/237142695_Physics_of_the_cold_fusion_phenomenon/links/541859700cf203f155ada963.pdf

[14]. T. Otomo, K. Ikeda, Dynamics of hydrogen in metals, *Radioisotopes* **63** (2014) 489-500. Also available from https://www.jstage.jst.go.jp/article/radioisotopes/63/10/63_489/_pdf/-char/ja

[15]. G.H. Miley, The IH UIUC Lab LENR Team, Study of a power source based on Low Energy Nuclear Reactions (LENRs) using hydrogen pressurized nanoparticles, Materials for Energy, Efficiency and Sustainability: TechConnect Briefs 2017. Also available from https://briefs.techconnect.org/wp-content/volumes/TCB2017v2/pdf/843.pdf.

[16]. M. Yamaguchi, Applied physical properties of metal hydrides, HESS (Hydrogen Energy System Society of Japan), Hydrogen Energy System, Vol.11, No.2 (1986) 11, 30-41. Also available from http://www.hess.jp/Search/data/11-02-030.pdf

[17]. G.H. Miley, The LENR Lab Team, Study of LENR for Space Power, *15th International Energy Conversion Engineering Conference*. Also available from http://dlb.isrc.ac.ir:8080/xmlui/bitstream/handle/isrc/1652184/6.2017-5035.pdf?sequence=1&isAllowed=y.

[18]. N. Koyama, O. Hatozaki, Comprehensive report-current status and future of cold fusion research-nuclear fusion induced by electrochemical reactions, *Appl. Phys.* 60 (1991) 220-226. Also available from https://www.jstage.jst.go.jp/article/oubutsu1932/60/3/60_3_220/_pdf.

[19]. T.Aruga, Hydrogen absorption and hydrogenation by palladium, *Surface Sci.* **27** (2006) 341—347. Also available from https://www.jstage.jst.go.jp/article/jsssj/27/6/27_6_341/_pdf/-char/ja.

[20]. K. Aoki, A. Machida, A. Ohmura, T. Watanuki, Frontier of high-pressure research on metal hydrides, **18** (2008) 273-278. Also available from https://www.jstage.jst.go.jp/article/jshpreview/18/3/18_3_273/_pdf.

[21]. J. Abe, R. Hanada, H. Kimura, Study of hydrogen and deuterium precipitation process in palladium by resistivity measurement, *J. Jpn. Inst. Metals*, **55** (1991) 254-259. Also available from https://www.jstage.jst.go.jp/article/jinstmet1952/55/3/55_3_254/_pdf.

[22]. N. Hasegawa, K. Kunimatsu, T. Ohi and T. Terasawa, Observation of excess heat during electrolysis of 1M LiOD in a fuel cell type closed cell, *Fourth International Conference on Cold Fusion*, 1993, Lahaina, Maui: Also available from http://coldfusioncommunity.net/pdf/lenr-canr/HasegawaNobservatioa.pdf.

[23]. M. Mckubre, F. Tanzella, P. Hagelstein, K. Mullican, M. Trevithick, The need for triggering in cold fusion reactions, *Proc. 10th International Conference on Cold Fusion*, Cambridge, MA, USA, 2003, pp. 199–212.

[24]. M. McKubre, F. Tanzella, The need for triggering in cold fusion reactions, *10th International Conference on Cold Fusion*, 2003, Cambridge, MA, USA. Available from https://www.researchgate.net/publication/241489694_The_Need_for_Triggering_in_Cold_Fusion_Reactions.

[25]. J. Va'vra, ON a possibility of existence of new atomic levels, which were neglected theoretically and not measured experimentally. Available from https://www.slac.stanford.edu/~jjv/activity/DDL/1_st_talk_siegen.pdf.

[26]. A. Meulenberg, K. P. Sinha, EDOs, *J. Condens. Matter Nucl. Sci.* **13** (2014) 368–377. Also available from http://coldfusioncommunity.net/wp-content/uploads/2018/07/368_JCMNS-Vol13.pdf.

[27]. [27] J. Va'vra, A simple argument that small hydrogen may exists, *Phys. Lett. B*, **794** (2019) 130-134. Also available from https://www.sciencedirect.com/science/article/pii/S0370269319303624 https://arxiv.org/ftp/arxiv/papers/1906/1906.08243.pdf

[28]. J.L. Paillet, On highly relativistic deep electrons, *J. Condens. Matter Nucl. Sci.* **29** (2019) 472–492. Also available from https://www.vixra.org/pdf/1902.0398v1.pdf.

[29]. [29] J.-L. Paillet, A. Meulenberg, Basis for EDOs of the hydrogen atom, *Proc. 19th International Conference on Condensed Matter Nuclear Science*, Padua, Italy, 13-17 April 2015. Also available from https://www.researchgate.net/profile/Jean-Luc_Paillet/publication/281089882_Basis_for_Electron_Deep_Orbits_of_the_Hydrogen_Atom/links/55d4482d08ae7fb244f5a40a/Basis-for-EDOs-of-the-Hydrogen-Atom.pdf.

[30]. J. Maly and J. Va'vra, Electron transitions on deep Dirac levels I, *Fusion Technol.*, 24 (1993) 307-318. Also available from https://www.tandfonline.com/doi/abs/10.13182/FST93-A30206.

[31]. J. A. Maly, J. Vavra, Electron transitions on deep Dirac levels II, *Fusion Technol.* 27 (1995) 59-70. Also available from https://www.tandfonline.com/doi/abs/10.13182/FST95-A30350?journalCode=ufst19.

[32]. J. Va'vra, On a possibility of existence of new atomic levels, which were neglected theoretically and not measured experimentally, presented at Siegen University, Germany, November 25, 1998. Available

from https://www.slac.stanford.edu/~jjv/activity/DDL/1_st_talk_siegen.pdf.
[33]. J. Va'vra, A new way to explain the 511 keV signal from the center of the Galaxy and some dark matter experiments, ArXiv: 1304.0833v12 [astro.ph-IM] Sept. 28, 2018. Available from https://www.slac.stanford.edu/~jjv/activity/dark/Vavra_small_hydrogen_atom_2018.pdf.
[34]. J.-L. Paillet, A. Meulenberg, Highly relativistic deep electrons and the Dirac equation, *J. Cond. Matter Nucl. Sci.* 33 (2020) 278–295. Also available from https://www.academia.edu/41956585/Highly_relativistic_deep_electrons_and_the_Dirac_equation.
[35]. Z.L. Zhang, W.S. Zhang, Z.Q. Zhang, Further study on the solution of schrödinger equation of hydrogen-like atom, *Proc. 9th International Conference on Cold Fusion*, May 21-25, 2002, Beijing, China, pp. 435-438. Available from https://www.lenr-canr.org/acrobat/ZhangZLfurtherstu.pdf.
[36]. J.L. Paillet, A. Meulenberg, EDOs of the hydrogen atom, *J. Condens. Matter Nucl. Sci.* **22** (2016) 1–23. Also available from https://www.researchgate.net/publication/312488578_Electron_Deep_Orbits_of_the_Hydrogen_Atom.
[37]. A. Meulenberg, Deep-orbit-electron radiation absorption and emission, Available From https://mospace.umsystem.edu/xmlui/bitstream/handle/10355/36501/DeepOrbitElectronRadiationAbstract.pdf?sequence=1&isAllowed=y.
[38]. A. Meulenberg, J.L. Paillet, Implications of the EDOs for cold fusion and physics–deep-orbit-electron models in LENR: Present and Future, *J. Condens. Matter Nucl. Sci. 24* (2017) 214–229, Also available from http://coldfusioncommunity.net/pdf/jcmns/v24/214_JCMNS-Vol24.pdf.
[39]. T. Yamamoto, D. Zeng, T. Kawakami, V. Arcisauskaite, K. Yata, M.A. Patino, N. Izumo, J.E. McGrady, H. Kageyama, M.A. Hayward, The role of π-blocking hydride ligands in a pressure-induced insulator-to-metal phase transition in SrVO2H, Nature Comm. 8 (2017). Also available from https://repository.kulib.kyoto-u.ac.jp/dspace/bitstream/2433/227748/1/s41467-017-01301-0.pdf https://www.jst.go.jp/pr/announce/20171031/index.html
[40]. E. CAMPARI, S. FOCARDI, V. GABBANI, V. MONTALBANO, F. PIANTELLI, S. VERONESI, OVERVIEW OF H-NI SYSTEMS: OLD EXPERIMENTS AND NEW SETUP, 5th Asti Workshop on Anomalies in Hydrogen-Deuterium-Loading Metals, Asti, Italy (2004), Available from, http://newenergytimes.com/v2/library/2004/2004CampariEGoverviewOfH-NiSystems.pdf
[41]. Sören Schlichting, Björn Schenke, The shape of the proton at high energies, Physics Letters B, Volume 739, 12 December 2014, Pages 313-319 Available from https://www.sciencedirect.com/science/article/pii/S0370269314008016
[42]. J. Abe, R. Hanada, H. Kimura, Study of hydrogen and deuterium precipitation process in palladium by resistivity measurement, *J. Jpn. Inst. Metals*, 55 (1991) 254-259. Also available from https://www.jstage.jst.go.jp/article/jinstmet1952/55/3/55_3_254/_pdf.
[43]. Michael C. H. McKubre, Review of experimental measurements involving measurements involving dd reactions, Presented at the Short Course on LENR for ICCF—10 August 25, 2003, Also available from https://www.lenr-canr.org/acrobat/McKubreMCHreviewofex.pdf
[44]. T. Mizuno, T. Ohmori, T. Akimoto, A. Takahasha, Production of heat during plasma electrolysis in liquid, *Jpn. J. Appl. Phys.* 39 (2000) 6055–6061. Also available from https://www.lenr-canr.org/acrobat/MizunoTproduction.pdf.
[45]. Kyodo International, INC., Nanoimprint lithography total solution: from mold to imprint services. Available from https://www.kyodo-inc.co.jp/english/electronics/nanoimprint/index.html.
[46]. J.P. Biberian, Biological transmutations: historical perspective, *J. Condens. Matter Nucl. Sci.* **7** (2012) 11–25. Also available from https://newenergytreasure.files.wordpress.com/2013/11/bacteria-jean-paul-biberian.pdf.
[47]. A. Meulenberg, Femto-atoms and transmutation, *17th Int. Conf. on Condensed Matter Nuclear Science (ICCF-17)*, Daejeon, 2012. Also available from http://coldfusioncommunity.net/wp-content/uploads/2018/07/346_JCMNS-Vol13.pdf.
[48]. Potassium channels. Available from http://pdb101.rcsb.org/motm/38.
[49]. Gap junction. Available from https://en.wikipedia.org/wiki/Gap_junction.
[50]. Na^+/K^+ATPase. Available from https://en.wikipedia.org/wiki/Na%2B/K%2B-ATPase.
[51]. Japanese Patent Application No. 2020-123285
[52]. Japanese Patent Application No. 2021-9701